

XMM-Newton and Suzaku analysis of the Fe K complex in the Seyfert 1 galaxy Mrk 509

G. Ponti^{1,2,3*}, M. Cappi², C. Vignali³, G. Miniutti^{1,4}, F. Tombesi^{2,3}, M. Dadina^{2,3}, A.C. Fabian⁵, P. Grandi², J. Kaastra^{6,7}, P.O. Petrucci⁸, S. Bianchi⁹, G. Matt⁹, L. Maraschi¹⁰ and G. Malaguti²

¹APC Université Paris 7 Denis Diderot, 75205 Paris Cedex 13, France

²INAF–IASF Bologna, Via Gobetti 101, I–40129, Bologna, Italy

³Dipartimento di Astronomia, Università di Bologna, Via Ranzani 1, I–40127, Bologna, Italy

⁴Laboratorio de Astrofísica Espacial y Física Fundamental (CAB-CSIC-INTA), Postal Address:

LAEFF, European Space Astronomy Center, P.O. Box 78, E-28691 Villanueva de la Cañada, Madrid

⁵Institute of Astronomy, Madingley Road, Cambridge CB3 0HA

⁶SRON Netherlands Institute for Space Research, Sorbonnelaan 2, 3584 CA Utrecht, The Netherlands

⁷Astronomical Institute, University of Utrecht, Postbus 80000, 3508 TA Utrecht, The Netherlands

⁸Laboratoire d’Astrophysique de Grenoble-Université Joseph–Fourier/CNRS UMR 5571 –BP 53, F–38041 Grenoble, France

⁹Dipartimento di Fisica, Università degli Studi Roma Tre, via della Vasca Navale 84, 00146 Roma, Italy

¹⁰INAF/Osservatorio Astronomico di Brera, Via Brera 28, 20121, Milano, Italy

1 November 2018

ABSTRACT

We report on partially overlapping *XMM-Newton* (~ 260 ks) and *Suzaku* (~ 100 ks) observations of the iron K band in the nearby, bright Seyfert 1 galaxy Mrk 509. The source shows a resolved neutral Fe K line, most probably produced in the outer part of the accretion disc. Moreover, the source shows further emission blue-ward of the 6.4 keV line due to ionized material. This emission is well reproduced by a broad line produced in the accretion disc, while it cannot be easily described by scattering or emission from photo-ionized gas at rest. The summed spectrum of all *XMM-Newton* observations shows the presence of a narrow absorption line at 7.3 keV produced by highly ionized outflowing material. A spectral variability study of the *XMM-Newton* data shows an indication for an excess of variability at 6.6–6.7 keV. These variations may be produced in the red wing of the broad ionized line or by variation of a further absorption structure. The *Suzaku* data indicate that the neutral Fe K α line intensity is consistent with being constant on long timescales (of a few years) and they also confirm as most likely the interpretation of the excess blueshifted emission in terms of a broad ionized Fe line. The average *Suzaku* spectrum differs from the *XMM-Newton* one for the disappearance of the 7.3 keV absorption line and around 6.7 keV, where the *XMM-Newton* data alone suggested variability.

Key words: galaxies: individual: Mrk 509 – galaxies: active – galaxies: Seyfert – X-rays: galaxies

1 INTRODUCTION

Deep investigations of the Fe K band in the brightest AGNs allow us to probe the presence of highly ionized emitting/absorbing components from the innermost regions around the central black hole. The high-sensitivity X-ray satellites *XMM-Newton* and *Chandra* have shown that the presence of a narrow core of the lowly ionized Fe K α line is nearly ubiquitous (Yaqoob & Padhmanaban 2004;

Guainazzi et al. 2006; Nandra et al. 2007) and that ionized components of the line, generally associated with emission from photo- and/or collisionally- ionized distant gas are also common (NGC 5506, NGC 7213, IC 4329A; Bianchi et al. 2003; Page et al. 2003; Reynolds et al. 2004; Ashton et al. 2004; Longinotti et al. 2007; see also Bianchi et al. 2002; 2005). The presence of broad (neutral or ionized) components of Fe K lines can only be tested via relatively long exposures of the brightest sources (e.g., Guainazzi et al. 2006; Nandra et al. 2007). Moreover, the observational evidence for broad lines and their interpretation in terms of relativistic

* ponti@iasfbo.inaf.it

effects may be questioned when an important absorbing ionized component is present. Spectral variability studies help in disentangling the different, often degenerate, spectral components (Ponti et al. 2004; Iwasawa et al. 2004; Ponti et al. 2006; Tombesi et al. 2007; Petrucci et al. 2007; DeMarco et al., in prep.).

Mrk 509 ($z=0.034397$) is the brightest Seyfert 1 of the hard (2–100 keV) X-ray sky (Malizia et al. 1999; Revnivtsev et al. 2004; Sazonov et al. 2007) that is not strongly affected by a warm absorber component (Pounds et al. 2001; Yaqoob et al. 2003). The HETG *Chandra* observation confirms the presence of a narrow component of the Fe K line with an equivalent width (EW) of 50 eV (Yaqoob et al. 2004). The presence of a second ionized component of the Fe K line at 6.7–6.9 keV has been claimed by Pounds et al. (2001) who fitted it using a relativistic profile, but Page et al. (2003) showed that the same spectral feature was consistent also with a simple Compton reflection component from distant material. The broad-band *BeppoSAX* spectrum and, in particular, the soft excess, have been fitted by De Rosa et al. (2004) with a reflection component from a ionized disc in addition to a neutral reflection component. Finally, Dadina et al. (2005) found evidence of absorption due to transient, relativistically red–blue–shifted ionized matter.

Here we present the spectral and variability analysis of the complex Fe K band of Mrk 509, using the whole set of *XMM-Newton* and *Suzaku* observations. The paper is organized as follows. Section 2 describes the observations and the data reduction. In Sect. 3 the spectral analysis of the EPIC-pn data of the Fe K band (using phenomenological models) is presented. In particular in Sect. 3.3, to check for the presence of an absorption line, the EPIC-MOS data have also been considered. In Sect. 3.4 the spectral variability analysis, within the *XMM-Newton* observations, is presented. Sect. 4 describes the spectral analysis of the Fe K band of the *Suzaku* summed (XIS0+XIS3) data and the detailed comparison with the spectrum accumulated during the *XMM-Newton* observations. In Sect. 4.1 the HXD-pin data are introduced in order to estimate the amount of reflection continuum present in the source spectrum. Finally, a more physically self-consistent fit of the EPIC spectra of all the EPIC instruments (EPIC-pn plus the two EPIC-MOS) is investigated in Sect. 5. The results of our analysis are discussed in Sect. 6, followed by conclusions in Sect. 7.

2 OBSERVATIONS AND DATA REDUCTION

Mrk 509 was observed 5 times by *XMM-Newton* on 2000–10–25, 2001–04–20, 2005–10–16, 2005–10–20 and 2006–04–25. All observations were performed with the EPIC-pn CCD camera operating in small window observing mode and with the thin filter applied. The total pn observation time is of about 260 ks. Since the live-time of the pn CCD in small window mode is 71 per cent, the net exposure of the summed spectrum is of about 180 ks. The analysis has been made with the SAS software (version 7.1.0), starting from the ODF files. Single and double events are selected for the pn data, while only single events are used for the MOS camera because of a slight pile-up effect. For the pn data we checked that the results obtained using only single events (that allow a superior energy resolution) are consistent with those from the MOS, finding good agreement. The source and background photons are extracted from a region of 40 arcsec within the same CCD of the source both for the pn and MOS data. Response matrices were generated using the SAS tasks RMFGEN and ARFGEN.

Suzaku observed Mrk 509 four times on 2006–04–25, 2006–10–14, 2006–11–15 and 2006–11–27. The last *XMM-Newton* and

the first *Suzaku* observations overlap over a period of ~ 25 ks. Event files from version 2.0.6.13 of the *Suzaku* pipeline processing were used and spectra were extracted using XSELECT. Response matrices and ancillary response files were generated for each XIS using XISRMFGEN and XISSIMARFGEN version 2007–05–14. The XIS1 camera data are not considered here because of the relatively low effective area in the Fe K energy interval, while the XIS2 is unavailable for observations performed after November 2006. We used the data obtained during the overlapping interval to check whether the EPIC pn and MOS data on one hand and the *Suzaku* XIS0 and XIS3 data on the other hand are consistent within the inter-calibration uncertainties. We found an overall good agreement between the data from the two satellites, the parameters related to the main iron emission features and the power-law continuum being the same within the errors (except for the XIS2 camera above 8 keV). The total XIS observation time is about 108 ks. The source and background photons are extracted from a region of 4.3 arcmin within the same CCD of the source. For the HXD/PIN, instrumental background spectra and response matrices provided by the HXD instrument team have been used. An additional component accounting for the CXB has been included in the spectral fits of the PIN data.

All spectral fits were performed using the Xspec software (version 12.3.0) and include neutral Galactic absorption ($4.2 \times 10^{20} \text{ cm}^{-2}$; Dickey & Lockman 1990), the energies are rest frame if not specified otherwise, and the errors are reported at the 90 per cent confidence level for one interesting parameter (Avni 1976). The sum of the spectra has been performed with the MATHPHA, ADDRMF and ADDARF tools within the HEASOFT package (version 6.1).

3 FE K BAND EMISSION OF MRK 509: THE *XMM-Newton* DATA

The primary goal of this investigation is the study of the Fe K line band; therefore, in order to avoid the effects of the warm absorber (although not strong; Yaqoob et al. 2003; Smith et al. 2007) and of the soft excess, we concentrate on the analysis of the data in the 3.5–10 keV band only. A detailed study of the warm absorber and its variations will be performed by Detmers et al. (in prep), we can nevertheless anticipate that the warm absorber has negligible effect in the Fe K energy band and thus on the results presented here. Figure 1 shows the source light curve in the 3.5–10 keV energy band obtained from the *XMM-Newton* pointings. Mrk 509 shows variations of the order of ~ 30 per cent over the different observations, while almost no variability is detected within each observation. Only during the fourth observation the source shows significant variability, with a mean fractional rms of about 0.04.

We start the analysis of the *XMM-Newton* data considering the spectra from the EPIC-pn camera only (including the EPIC-MOS data only when a check of the significance of a feature is required; see Sect. 3.3). We have fitted a simple power law model to the 3.5–10 keV data and found that the spectral index steepens with increasing flux. It goes from 1.54 ± 0.03 to 1.72 ± 0.03 for fluxes of 2.5×10^{-11} and $3.3 \times 10^{-11} \text{ erg cm}^{-2} \text{ s}^{-1}$, respectively ($3.0 \times 10^{-11} - 4.3 \times 10^{-11} \text{ erg cm}^{-2} \text{ s}^{-1}$, in the 2–10 keV band). We firstly phenomenologically fitted the Fe K complex of each single observation with a series of emission-absorption lines (see also §3.3) and checked that the results on the parameters of Fe K complex obtained in each observation are consistent within the errors (not a surprising result in light of the low statistics of the single

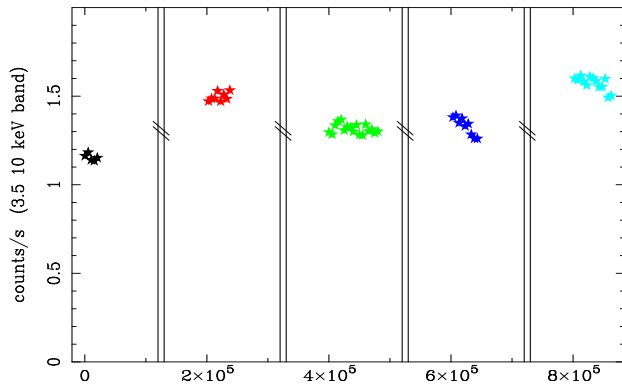


Figure 1. 3.5–10 keV EPIC–pn light curves of the *XMM-Newton* observations. The abscissa shows the observation time in seconds. The time between the different observations is arbitrary. The black, red, green, blue and light blue show the light curves during the 2000–10–25, 2001–04–20, 2005–10–16, 2005–10–20 and 2006–04–25 observations, respectively.

spectra and weakness of the ionized features; see § 3.4). Hence, we concluded that the continuum variations do not strongly affect the observed shape of the narrow–band emission/absorption structures in the Fe K band. Thus, in order to improve the signal–to–noise ratio and thus to detail the fine structures of the Fe K band, the spectra of all the *XMM-Newton* observations have been summed (see §3.4 for the study of the source spectral variability). The summed mean EPIC–pn spectrum has been grouped in order to have at least 1000 counts in each data bin. Moreover, this binning criterion ensures to have at least 30 data–points per keV in the 4–7 keV band, where the Fe $K\alpha$ complex is expected to contribute. This guarantees a good sampling of the energy resolution of the instrument and the possibility of fully exploiting the spectral potentials of the EPIC instruments. Fig. 2 shows the ratio between the data and the best–fit power law. The energy band used during the fit has been restricted to 3.5–5 and 8–10 keV, in order to avoid the Fe K band, hence measuring the underlying continuum. The resulting best–fit power–law continuum has a photon index of 1.63 ± 0.01 and very well reproduces the source emission ($\chi^2=170.0$ for 163 degrees of freedom, dof) outside the Fe K band. The inclusion of the Fe K band shows that other components are necessary to reproduce it ($\chi^2=753.9$ for 307 dof). The bad statistical result is explained by the presence of clear spectral complexity in the 6–7 keV band.

3.1 The 6.4 keV emission line

Panel a of Fig. 2 shows the clear evidence for a prominent emission line, consistent with a neutral Fe $K\alpha$ line at 6.4 keV. We therefore added a Gaussian emission line to the model, obtaining a very significant improvement of the fit ($\Delta\chi^2=392.1$ for the addition of 3 dof). The best–fit energy of the line is 6.42 ± 0.02 keV, consistent with emission from neutral or slightly ionised material. The line has an equivalent width of 69 ± 8 eV and is clearly resolved ($\sigma=0.12 \pm 0.02$ keV), as shown by the contour plot in the left panel of Fig. 3. The residuals in panel b of Fig. 2 show no excess redward of this emission line, which could have been indicative of emission from relativistically redshifted neutral material.

3.2 The ionized Fe K emission line

An excess is, however, present in the range 6.5–7 keV (Fig. 2, panel a). If modeled with a Fe $K\beta$ component with the expected energy

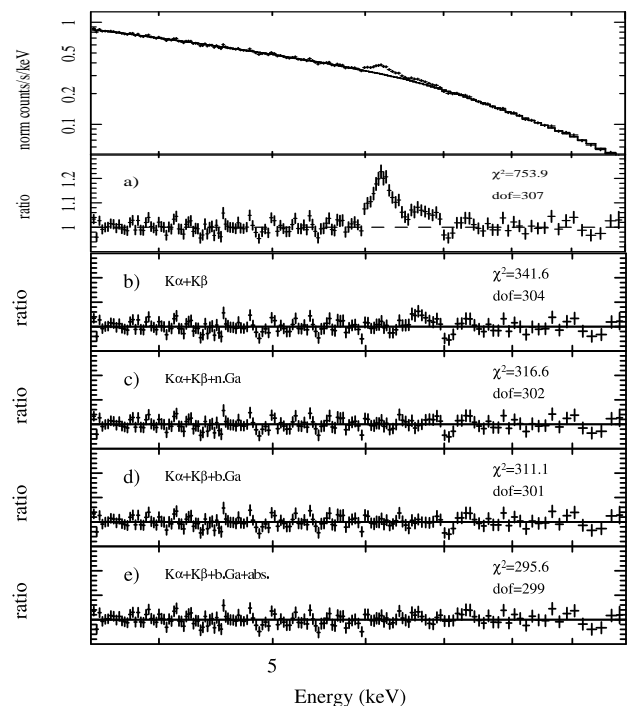


Figure 2. (*Upper panel*) Observed–frame 3.5–10 keV summed *XMM-Newton* EPIC–pn spectrum fitted in the 3.5–5 and 8–10 keV band with a power law. (*Panel a*) Data/model ratio. This ratio shows a clear evidence for a neutral Fe K emission line and further emission from ionized Fe, as well as other complexities around 7 keV. (*Panel b*) Data/model ratio when two resolved emission lines (for the Fe $K\alpha$ and $K\beta$) are included in the spectral fitting. Strong residuals are still present, indicative of ionized Fe K emission, while no residual emission redward of the neutral Fe K line appears. (*Panel c*) Data/model ratio when a narrow emission line is included in the model to reproduce the ionized emission. (*Panel d*) Same as panel c, but with a single broad emission line instead of a narrow line. In both cases (panel c and d), an absorption feature is present around 7 keV. (*Panel e*) Data/model ratio when an absorption component (modeled using *XSTAR*) and a relativistic ionized line are added to the power law and the emission from neutral Fe K.

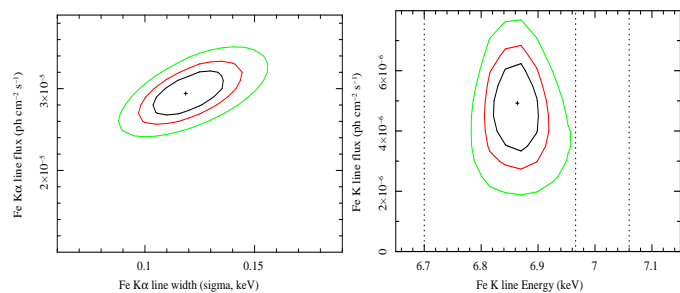


Figure 3. (*Left panel*) Contour plot of the sigma vs. intensity of the neutral Fe K line. (*Right panel*) Contour plot of the energy vs. intensity of the narrow line used to fit the ionized Fe K emission. The narrow line energy is not consistent with emission from Fe XXV (neither with the forbidden at 6.64 keV, nor with the resonant at 6.7 keV), Fe XXVI or Fe $K\beta$, whose energy is indicated by the vertical dotted lines (from left to right).

(fixed at 7.06 keV) and forced to have an intensity of 0.15 of the $K\alpha$ (Palmeri et al. 2003a,b; Basko 1978; Molendi et al. 2003) and a width equal to the Fe $K\alpha$ line (i.e. assuming that the $K\alpha$ and $K\beta$ line originate from one and the same material), the fit improves significantly ($\Delta\chi^2=20.3$). Nonetheless, significant residuals are still present in the 6.5–6.9 keV band (panel b of Fig. 2). If this further excess is modelled with a narrow Gaussian line ($\Delta\chi^2=25$ for 2 additional dof), the feature ($EW=12\pm 4$ eV) is found to peak at $E=6.86\pm 0.04$ keV (see panel c of Fig. 2 and right panel of Fig. 3). Thus, the energy centroid is not consistent with the line being produced by either Fe XXV or Fe XXVI (right panel of Fig. 3) in a scattering medium distant from the X-rays source (Bianchi et al. 2002; 2004). The higher energy transition of the Fe XXV complex is the "resonant line" expected at 6.7 keV (see e.g. Bianchi et al. 2005). Thus, to save this interpretation, it is required that the photo-ionized gas has a significant blueshift (~ 5700 km/s, if the line is associated to Fe XXV) or redshift (~ 4500 km/s, for Fe XXVI). Then, instead of fitting the ionized excess with a single line, we fitted it with two narrow lines forcing their energies to be 6.7 and 6.96 keV. The fit clearly worsens ($\chi^2=326.7$ for 302 dof, corresponding to a $\Delta\chi^2 = -10.1$ for the same dof). However, if the gas is allowed to be outflowing, the fit improves ($\Delta\chi^2=4.3$ for the addition of 1 new parameter; $\chi^2=312.3$ for 301 dof; the EW are 8.9 and 12.4 eV for the Fe XXV and Fe XXVI lines, respectively) as respect to the single narrow emission line and it results to have a common velocity of 3500^{+1900}_{-1200} km/s.

Alternatively, the excess could be produced by a single broad line coming from matter quite close to the source of high-energy photons (in this case the Fe K emission is composed by Fe $K\alpha+\beta$ plus another Fe K line). Leaving the width of the line free to vary, the fit improves, with $\chi^2=311.1$ (panel d Fig. 2) and $\Delta\chi^2$ of 5.5, with respect to the single narrow ionized emission line fit, and $\Delta\chi^2$ of 1.3 for the same dof with respect to the best-fit model with two narrow ionized lines. The resulting broad ionized Fe K line has $EW=23\pm 9$ eV and $\sigma=0.14^{+0.13}_{-0.08}$ keV. The best-fit energy of the line does not change significantly ($E=6.86^{+0.08}_{-0.16}$ keV); however, in this case the emission is consistent (at the 99 per cent confidence level) with either Fe XXV or Fe XXVI. Although the statistical improvement is not highly significant, in the following we will consider that the ~ 6.8 –6.9 keV excess is indeed associated with a resolved emission line.

3.3 Ionized absorption?

The *XMM-Newton* data also display a narrow absorption feature at $E\sim 7$ keV (observed frame; see Fig. 2, panel d). Since this feature is very close to the broad excess we just discussed, its significance and intensity are degenerate with the broad emission-line parameters. In order to gain some insight, we then fixed the broad emission-line parameters at the best-fit ones obtained before the addition of a narrow (σ fixed at 1 eV) Gaussian absorption line component. In this case, the line is significant at the ~ 99 per cent confidence level (dashed contours of Fig. 4; $\Delta\chi^2=15.5$ for 2 additional parameters; see also panel e of Fig. 2). Once the MOS data¹ are added, the significance of this feature increases to 99.9 per cent (solid contours of Fig. 4), in both cases, of a broad and of a narrow ionized emission line. The best fit energy and EW of the line are $E=7.28^{+0.03}_{-0.02}$ keV

¹ The shapes of the emission/absorption lines in the MOS instruments appear slightly narrower, although consistent with the values obtained with the pn instrument.

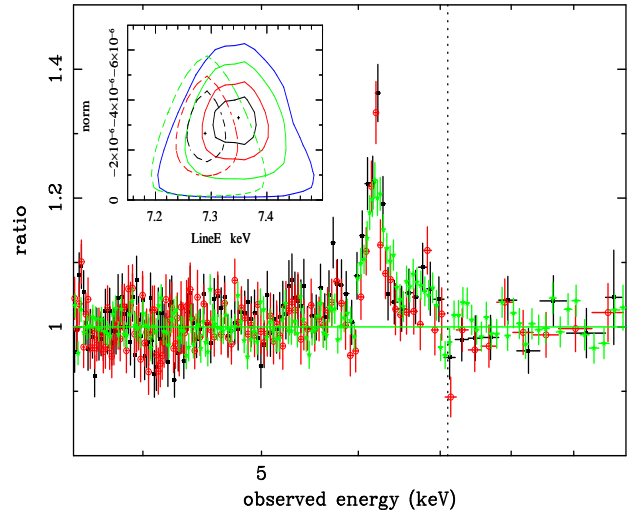


Figure 4. Superposition of the pn (green), MOS1 (black) and MOS2 (red) summed spectra of all the *XMM-Newton* observations. The data are fitted, in the 3.5–5 and 8–10 keV bands with a power law, absorbed by Galactic material. The same structures are present in the three spectra. In particular, a narrow drop of emission is present in all the instruments at the same energy (see vertical dotted line). (Inset panel) Confidence contour plot of the intensity vs. energy of the narrow unresolved ionized absorption when using the pn data alone (dashed contours) and including the MOS data as well (solid contours). The lines indicate the 68.3 (black), 90 (red), 99 (green) and 99.9 (blue) per cent confidence levels.

and $EW=-14.9^{+5.2}_{-5.5}$ eV, $E=7.33^{+0.03}_{-0.04}$ keV and $EW=-13.1^{+5.9}_{-2.9}$ eV, in the pn alone and in the pn+MOS, respectively.

3.4 Time resolved spectral variability and total rms spectrum

One of the goals of the present analysis is to search for time-variation of the emission/absorption features of the Fe K complex. To measure possible variations in the Fe K band, the mean EPIC-pn spectra of each of the 5 *XMM-Newton* observations have been studied. The spectra are fitted with the same model composed by a power law plus three emission lines for the Fe $K\alpha$, $K\beta$ (with the width fixed at the best-fit value, $\sigma=0.12$ keV) and the broad ionized Fe K line. The low statistics of the spectra of the single observations prevents us from the detection of significant spectral variability of the weak ionised emission/absorption lines. The neutral Fe K line is better constrained and we find that its EW is anti-correlated with the level of the continuum, as expected for a constant line.

A different, more sensitive, way to detect an excess of spectral variability is the total rms function. The upper panel of Fig. 5 displays the shape of the summed spectrum in the Fe K line band. The lower panel shows the total rms spectrum (Revnitsev et al. 1999; Papadakis et al. 2005) calculated with time bins of ~ 4.5 ks. The total rms is defined by the formula:

$$RMS(E) = \frac{\sqrt{S^2(E) - \langle \sigma_{err}^2 \rangle}}{\Delta E * arf(E)} \quad (1)$$

where S^2 is the source variance in a given energy interval ΔE ; $\langle \sigma_{err}^2 \rangle$ is the scatter introduced by the Poissonian noise and arf is the telescope effective area convolved with the response matrix².

² The total rms spectrum provides the intrinsic source spectrum of the variable component. Nevertheless, we measure the variance as observed

This function shows the spectrum of the varying component only, in which any constant component is removed and has been computed by using the different *XMM-Newton* observations as if they were contiguous. The total rms spectrum may be reproduced by a power law with a spectral index of 2.13 ($\chi^2=46.4$ for 43 dof). Thus, the variable component is steeper than the observed power law in the mean spectrum, in agreement with the mentioned observed steepening of the photon index (Γ) with flux. The Γ -flux correlation is commonly observed in Seyfert galaxies and has been interpreted as being due to the flux-correlated variations of the power-law slope produced in a corona above an accretion disc and related to the changes in the input soft seed photons (e.g. Haardt, Maraschi & Ghisellini 1997; Maraschi & Haardt 1997; Poutanen & Fabian 1999; Zdziarski et al. 2003). These models predict the presence of a pivot point, that would correspond to a minimum in the total rms spectrum. The observation of a perfect power law shape (see Fig. 5) indicates that the pivot point (if present) has to be outside the 3–10 keV energy band. On the other hand, the slope-flux behaviour can be explained in terms of a two-component model (McHardy, Papadakis & Uttley 1998; Shih, Iwasawa & Fabian 2002) in which a constant-slope power law varies in normalization only, while a harder component remains approximately constant, hardening the spectral slope at low flux levels only, when it becomes prominent in the hard band. In this scenario the spectral index of the variable component is equal to the one of the total rms spectrum, that is $\Gamma=2.13$.

Moreover we note that at the energy of the neutral and ionized Fe K line components, no excess of variability is present, in agreement with these components being constant, while an indication for an excess of variability is present around 6.7 keV. In order to compute the significance of this variability feature, a narrow Gaussian line has been added to the modelling of the total rms spectrum. The best-fit energy of the additional line is 6.69 keV, with a σ fixed at the instrumental energy resolution, while the resulting $\Delta\chi^2$ is 8.9 for the addition of 2 parameters (that corresponds to an F-test significance of 98.8 per cent). Introducing the line, the continuum spectral index steepens to $\Gamma \sim 2.18$. The dashed line in Fig. 5 highlights the centroid energy of the neutral Fe K α line, while the dotted line (at ~ 6.7 keV, rest frame) is placed at the maximum of the variability excess. This energy corresponds to a drop of emission in the real spectrum, as we shall discuss in more detail in Section 5.

4 THE *Suzaku* VIEW OF THE FE K BAND EMISSION

As mentioned in §2, the source was also observed with *Suzaku*. The first 25 ks *Suzaku* observation is simultaneous with the last *XMM-Newton* pointing. The source spectra of all the instruments are in very good agreement, during the simultaneous observation. The spectrum is also consistent with the presence of the emission and absorption lines, as observed in the mean *XMM-Newton* spectrum, nevertheless, due to the low statistics of the 25 ks spectrum and the weakness of the ionized features, it is not possible to perform a detailed comparison. Only the presence of the strong Fe K α line can be investigated, the ionized emission and absorption lines are not constrained in the 25 ks *Suzaku* exposure.

through the instrument. Thus, the sharp features in the source spectrum, as well as the effects of the features on the effective area, are broadened by the instrumental spectral resolution. For this reason, to obtain the total rms spectrum, we take into account the convolution of the effective area with the spectral response.

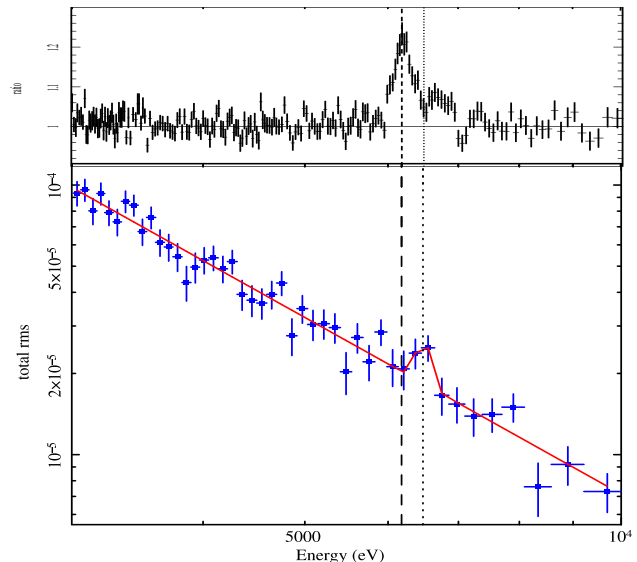


Figure 5. Lower panel: Total rms variability spectrum of the *XMM-Newton* observations. The data (blue crosses) show the spectrum of the variable component. The best-fit model is a power law with spectral index $\Gamma=2.18$ (red line) plus a Gaussian emission line (improving the fit by $\Delta\chi^2$ of 8.9 for the addition of 2 parameters). The dashed line highlights the centroid energy of the neutral Fe K α line, while the dotted line is placed at the maximum of the variability excess, modeled with the Gaussian emission line. The excess variability energy corresponds to a drop of emission of the real spectrum.

Also during the 4 *Suzaku* pointings, Mrk 509 has shown little variability, with flux changes lower than 10–15 per cent, hampering any spectral variability study. Fig. 6 shows the *XMM-Newton* (black) and *Suzaku* XIS0+XIS3 (red) summed mean spectra. The data were fitted, in the 3.5–5 and 7.5–10 keV bands, with a simple power law and Galactic absorption: the ratio of the data to the best fit model is shown in Fig. 6. The source emission varied between the *XMM-Newton* and the *Suzaku* observations. The best-fit spectral index and the 3.5–10 keV band fluxes are: $\Gamma=1.63\pm 0.01$ and $\Gamma=1.71\pm 0.02$ and 2.63×10^{-11} and 3.11×10^{-11} ergs cm $^{-2}$ s $^{-1}$, during the *XMM-Newton* and *Suzaku* observations, respectively. The neutral and ionized Fe K emission lines appear constant, while some differences are present at 6.7 keV, the same energy where the *XMM-Newton* data were suggesting an increase of variability. Other more subtle differences appears at ~ 7 keV, where the absorption line imprints its presence in the *XMM-Newton* data only.

The *Suzaku* spectrum of Mrk 509 shows, in good agreement with the *XMM-Newton* one, a resolved neutral Fe K line smoothly joining with a higher energy excess, most likely due to ionized iron emission (see Fig. 6). Given that no absorption lines around 6.7 keV or 7.3 keV are present in the *Suzaku* data, the spectrum may be useful to infer the properties of the emission lines more clearly.

The XIS0+XIS3 *Suzaku* summed spectrum has been fitted in the 3.5–10 keV band with a power law plus two resolved Gaussian emission lines to reproduce the emission from Fe K $\alpha+\beta$. The parameters of the Fe K α line are free to vary, while the Fe K β ones are constrained as in §3.2. This fit leaves large residuals ($\chi^2=1379.8$ for 1337 dof) in the Fe K band. In this respect, it is difficult to describe the >6.5 keV excess with a single narrow ionized Fe line (either due to Fe XXV or Fe XXVI). In fact, although the addition of a narrow line is significant ($\Delta\chi^2=20.1$ for 2 more parameters), it leaves residuals in the Fe K band. This remaining excess can

	3.5–10 keV	BEST-FIT	SPECTRA						
Suzaku									
	Γ	pl norm ^a	$E_{\text{Neut.}}$ keV	$\sigma_{\text{Neut.}}$ keV	$A_{\text{Neut.}}^{\text{b}}$ (EW) ^c	$E_{\text{Ion.}}$ keV	$\sigma_{\text{Ion.}}/r_{\text{in}}$ keV/ r_g	$A_{\text{Ion.}}^{\text{b}}$ (EW) ^c	χ^2/dof
A	1.72±0.02	1.12±0.02	6.42±0.03	<0.06	1.7±0.5 (32)	6.54±0.09	0.40±0.1	4.6±1.2 (90)	1344/1340
B	1.72±0.02	1.12±0.02	6.42±0.02	<0.07	2.1±0.5 (40)	6.61±0.08	24±10	3.4±0.8 (79)	1346/1340
Self-consistent model XMM-Newton									
	Γ	pl norm ^a	$E_{\text{Neut.}}$ keV	$\sigma_{\text{Neut.}}$ keV	$A_{\text{Neut.}}^{\text{b}}$	Incl. deg	ξ erg cm s ⁻¹	$A_{\text{Refl.Ion.}}^{\text{b}}$	
C	1.70±0.01	0.92±0.04	6.41±0.01	0.07±0.01	2.2±0.3	47±2	11 ⁺²⁰⁰ ₋₇	0.9 ^{+3.0} _{-0.5}	
	N_H^{d}	log(ξ)	z	χ^2/dof					
	5.8 ^{+5.2} _{-4.8}	5.15 ^{+1.25} _{-0.52}	-0.0484 ^{+0.012} _{-0.013}	894.3/876					

Table 1. *Top panel:* Best-fit values of the summed spectra (XIS0+XIS3) of all *Suzaku* observations fitted in the 3.5–10 keV band. Both model A and B include a power law and two Gaussian lines $K\alpha+\beta$ to fit the 6.4 keV excess. In addition to this baseline model, either another Gaussian component (Model A) or a DISKLINE profile (Model B) have been added to reproduce the ionized line, respectively. In Table the best-fit power law spectral index (Γ) and normalization as well as the Fe $K\alpha$ energy, width and normalization are reported for model A and B. The energy, width and normalization are reported when a Gaussian profile for the ionized Fe K line is considered (Model A), while the best fit energy, inner radius and normalization are presented when a DISKLINE profile is fitted (Model B). Standard disc reflectivity index, outer disc radius and disc inclination of $\alpha = 3$, $r_{\text{out}} = 400 r_g$ and 30° have been assumed for the relativistic profile. *Bottom panel:* Best fit results of the summed *XMM-Newton* EPIC-pn and EPIC-MOS data of Mrk 509 (fitted in the 3.5–10 keV band). The model (WABS*ZXIPCF*(POW+ZGAUS+ZGAUS+PEXRAV+KDBLUR*(REFLION))) consists of: i) a power law; ii) two Gaussian emission lines for the Fe $K\alpha$ and $K\beta$ emission (this latter has energy is fixed to the expected value, 7.06 keV, intensity and width tied to the $K\alpha$ values); iii) a neutral reflection continuum component (PEXRAV in Xspec) with $R=1$ (value broadly consistent with the pin constraints and the values previously observed; De Rosa et al. 2004), Solar abundance and high energy cut off of the illuminating power law at 100 keV; iv) a ionized disc reflection spectrum (*reflion* model; Ross & Fabian 2005) with the disc inner and outer radii and the emissivity of 6, 400 r_g and -3 , respectively. The best fit disc inclination and ionization and the normalization of the disc reflection component are shown; v) an ionized absorption component (ZXIPCF) totally covering the nuclear source. The best fit column density, ionization parameter and outflow velocity are reported. *a)* In units of 10^{-2} photons $\text{keV}^{-1} \text{cm}^{-2} \text{s}^{-1}$ at 1 keV; *b)* In units of 10^{-5} photons $\text{cm}^{-2} \text{s}^{-1}$; *c)* In units of eV; *d)* In units of 10^{22} atoms cm^{-2} .

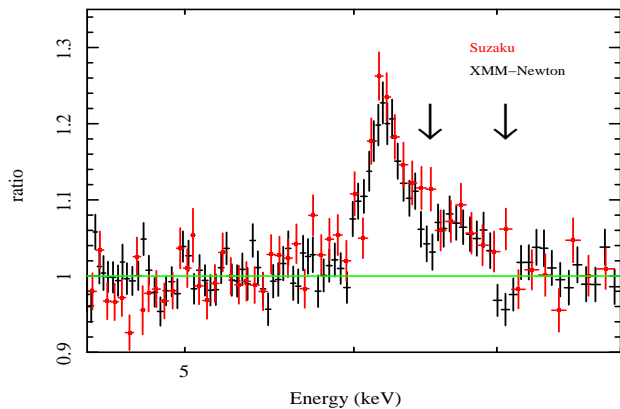


Figure 6. *XMM-Newton* (black) and *Suzaku* XIS0+XIS3 (red) summed spectra. The data are fitted, in the 3.5–5 and 7.5–10 keV bands, with a simple power law, absorbed by Galactic material, and the ratio of the data to the best fit model is shown. The arrows mark absorption features in the spectrum.

be reproduced ($\Delta\chi^2=5.9$ for 1 more parameter), in a photoionized gas scenario, by a blend of two unresolved ionized lines, requiring three emission lines to fit the Fe K band (Fe $K\alpha+\beta$, Fe XXV and Fe XXVI). In this case, such as in the analysis of the *XMM-Newton* mean spectrum, a blueshift of this component is suggested ($v=2600^{+2800}_{-2000}$ km s⁻¹). However, the best-fit model (this scenario is strengthened by the lack of narrow peaks) suggests that the excess may be in fact associated with a broad ionized Fe line (over which the ~ 6.7 keV and ~ 7.3 keV absorption lines are most likely superimposed, but during the *XMM-Newton* observation only). In fact considering a broad Fe line instead of the two narrow lines we

obtain an improvement of $\Delta\chi^2=9.7$ for the same dof (see Table 1, model A).

Thus, the *Suzaku* data indicate that the broad excess at 6.5–6.6 keV is indeed due to a broad line rather than a blend of narrow ionized Fe lines. Since broad lines may arise because of relativistic effects in the inner regions of the accretion flow, we tested this hypothesis by fitting the excess at 6.5–6.6 keV with a DISKLINE profile. The statistics of the spectrum is not such to allow us to constrain all the parameters of the ionized DISKLINE model. Thus, the disc reflectivity index has been fixed at the standard value ($\alpha = -3$, where the emissivity is proportional to r^α), the outer disc radius and inclinations to 400 gravitational radii (r_g) and 30° , respectively. The broad line is consistent with being produced in the accretion disc (Table 1, Model B); however, the emission from the innermost part of the disc is not required, the lower limit on the inner disc radius being 10–15 r_g . As clear from Fig. 6, the *Suzaku* data do not require any ionized Fe K absorption structures.

In order to quantify the differences between the *Suzaku* and *XMM-Newton* spectra (and, in particular, the reality of the absorption structures at 6.7 and 7.3 keV appearing in the *XMM-Newton* spectrum only) we fixed all the parameters of the *Suzaku* model (apart from the intensity and spectral index of the direct power law) and fit the *XMM-Newton* data with that model. This corresponds to assuming that the intrinsic line shapes do not vary between the two observations. Then, a narrow Gaussian line has been added to the *XMM-Newton* model to estimate the significance of the putative absorption structures. The improvement in the spectral fitting is evident, as indicated by the $\Delta\chi^2=28.3$ and 22 in the case of a line at $E=6.72\pm 0.04$ keV and $E=7.29\pm 0.04$ keV, respectively. The presence of these spectral features only in the *XMM-Newton* ob-

servations is thus indicative of variability at energies ~ 6.6 – 6.7 and ~ 7.3 keV.

4.1 The *Suzaku* pin data to constrain the reflection fraction

We add the pin data to measure the amount of reflection continuum. We note that the pin data provide a good quality spectrum up to 50 keV. The model used involves a direct power law plus a neutral reflection component (*pe xrav* model in *Xspec*; Magdziarz & Zdziarski 1995) plus the Fe $K\alpha+\beta$ resolved lines and a broad (DISKLINE) component of the line. As for model B we fix some of the parameters of the DISKLINE profile (disc inclination= 30° , $r_{out}=400 r_g$ and $\alpha=-3$). Moreover we assume a high-energy cut off of 100 keV and Solar abundance. Thus, by fitting the 3–50 keV band data, we obtained a reflection fraction $R = 0.4^{+0.6}_{-0.2}$ and a spectral index $\Gamma=1.76^{+0.12}_{-0.03}$. The total EW of the emission lines above the reflected continuum (about 1.2 keV) is broadly consistent with the theoretical expectations (Matt et al. 1996) and with what observed in Compton thick Seyfert 2 galaxies, where the primary continuum is absorbed and only the reflection is observed. Nevertheless, also for this source, as already known from previous studies (Zdziarski et al. 1999), we observe that the spectral index and the reflection fraction are degenerate and strongly depend on the energy band considered. In fact, if the 2–10 keV band is considered, the reflection fraction increases, resulting to be $R=1.1^{+0.2}_{-0.5}$ and the power-law photon index of $\Gamma=1.88^{+0.03}_{-0.02}$. The total EW of the Fe emission lines above the reflected continuum are about 750 eV. Again these values are broadly in agreement with expectations (Matt et al. 1996).

5 A PHYSICALLY SELF-CONSISTENT FIT: POSSIBLE ORIGIN OF THE SPECTRAL FEATURES

The analysis of the *XMM-Newton* and *Suzaku* data shows evidence for the presence of: i) a resolved, although not very broad, ($\sigma \sim 0.12$ keV) neutral Fe $K\alpha$ line and associated Fe $K\beta$ emission; ii) an ionized Fe K emission line inconsistent with emission from a distant scattering material at rest and most likely produced in the accretion disc; iii) an absorption line at ~ 7.3 keV, present in the summed spectrum of all *XMM-Newton* observations only; iv) an indication for an enhancement of variability - both by considering the *XMM-Newton* data alone and by comparison between the two data sets - at ~ 6.7 keV that could be either due to the high variability of the red wing of the broad ionized Fe K line, possibly associated with a variation of the ionisation of the disc, or to a second ionized absorption line.

These emission/absorption components are partially interconnected to each other given the limited CCD resolution onboard *XMM-Newton* and *Suzaku*. Thus we re-fit the *XMM-Newton* (both the pn and MOS in the 3.5–10 keV energy band) data with a model containing components that better describe the physical processes occurring in the AGN. In particular, we consider two Gaussian lines for the Fe $K\alpha$ and $K\beta$ emission plus a neutral reflection component (PEXRAV in XSPEC) with a reflection fraction $R = 1$ (consistent with the constraints given by the *Suzaku* pin data). The Fe $K\alpha$ line has an equivalent width of 1 keV above the reflection continuum. Moreover, we fit the broad ionized Fe K line with a fully self-consistent relativistic ionised disc reflection component (*reltline* model in *Xspec*; Ross & Fabian 2005, convolved with a LAOR kernel; KDBLUR in Xspec).

The statistics prevents us from constraining the parameters of

the relativistic profile. Standard values for the relativistic profile are assumed, with the disc inner and outer radii and the emissivity of 6, $400 r_g$, and -3 , respectively. Finally, the ~ 7.3 keV absorption line has been fitted with a photoionised absorption model (*zxcipcf* model in *Xspec*; Miller et al. 2007; Reeves et al. 2008; Model C, Table 1), assuming a total covering factor.

Table 1 shows the best-fit parameters. Once the presence of the reflection continuum is taken into account, the power law slope becomes steeper ($\Gamma=1.70\pm 0.01$, $\Delta\Gamma \sim 0.07$) as compared to the fit with a simple power law and emission absorption lines (see §3). The best fit energy of the neutral Fe $K\alpha$ line is $E=6.41\pm 0.01$ keV, consistent with being produced by neutral material, and results to be narrower ($\sigma=0.07\pm 0.01$ keV) than in the previous fits. The ionized emission line is fitted with a ionized disc reflection model. The only free parameters of such a component are the inclination and ionisation parameter of the disc that result to be $47\pm 2^\circ$ and $\xi=11^{+200}_{-7}$ erg cm s $^{-1}$ (Model C, Table 1). The material producing the 7.3 keV absorption feature in the *XMM-Newton* data has to be highly ionized, as also indicated by the absence of a strong continuum curvature. In fact, the best ionization parameter is $\log(\xi)=5.15^{+1.25}_{-0.52}$ and the column density $N_H = 5.8^{+5.2}_{-4.8} \times 10^{22}$ cm $^{-2}$. Nevertheless the observed energy of the absorption feature does not correspond to any strong absorption features, thus there is evidence for this absorption component to be outflowing with a shift $v = -0.0484^{+0.012}_{-0.013} c$ ($\sim 14000^{+3600}_{-4200}$ km s $^{-1}$). The resulting χ^2 is 894.3 for 876 dof.

6 DISCUSSION

This study clearly shows that long exposures are need to disentangle the different emitting/absorbing components contributing to the shape-variability of the Fe K complex in Seyfert galaxies. Here we discuss the origin of both neutral and ionized emission and absorption Fe lines in Mrk 509 which allow to have insights in the innermost regions of the accretion flow.

6.1 Neutral/lowly ionized Fe emission line

Once the broad ionized line is fitted, the width of the Fe $K\alpha$ line lowers to a value of 72 ± 11 eV (see Fig. 3) that corresponds to a $\text{FWHM}(\text{Fe } K\alpha)=8000\pm 1300$ km s $^{-1}$ (see Model C, Table 1). This value is slightly higher than that measured by Yaqoob & Padmanabhan with a ~ 50 ks HETG *Chandra* observation (2820^{+2680}_{-2800} km s $^{-1}$). The FWHM of the Fe $K\alpha$ line is larger than the width of the $H\beta$ line ($\text{FWHM}(H\beta)=3430\pm 240$ km s $^{-1}$; Peterson et al. 2004; Marziani et al. 2003), indicating that the Fe line is produced closer to the center than the optical BLR and, of course, than the torus postulated in unified models; we note that a wide range of FWHM values is observed for the BLR and the Fe K lines in local Seyfert galaxies (Nandra 2006). However, the UV and soft X-ray spectra of Mrk 509 show evidence for the presence of broad emission lines with FWHM of 11000 km s $^{-1}$ (Kriss et al. 2000). The origin of these UV and soft-X lines is still highly debated, nevertheless they may indicate that the BLR region is stratified, i.e. that these lines are not produced in the optical BLR but in the inner part of a stratified BLR region (see also Kaastra et al. 2002; Costantini et al. 2007), possibly as close as $2000 r_g$ from the center (about 0.012 pc, being the mass of the black hole in Mrk 509 $M_{BH} \simeq 1.43\pm 0.12 \times 10^8 M_\odot$ Peterson et al. 2004; Marziani et al. 2003). Nevertheless, if the line is produced in the innermost part

of a stratified BLR, it would require either a higher covering fraction or a higher column density than generally derived from the optical and ultraviolet bands. Simulations by Leahy & Creighton (1993) show that about 70 per cent of the sky, as seen by the central source, has to be covered in order to produce the Fe K α line, if the broad line clouds have column densities of about 10^{23} cm $^{-2}$, while the typical values for the BLR clouds covering fractions are of the order of 10–25 per cent (Davidson & Netzer 1979; Goad & Koratkar 1998). Alternatively, the Fe K α line may be produced by reflection by the outer part of the accretion disc.

6.2 Ionized Fe emission lines

The spectrum of Mrk 509 shows emission from ionized iron, consistent with either Fe XXV or Fe XXVI, implying photoionized gas outflowing or inflowing respectively. Alternatively, the ionized Fe K emission may be produced by reflection from the inner part of the accretion disc.

In fact, both the *XMM-Newton* and the *Suzaku* data are consistent with the two scenarios, even if a slightly better fit ($\Delta\chi^2=5.5$ and 9.7 for *XMM-Newton* and *Suzaku*, respectively) is obtained in the case of broad line. Moreover in the case of narrow emission lines the emitting gas should have a significant outflow (for Fe XXV, $v\sim 3500$ and 2600 km s $^{-1}$ for *XMM-Newton* and *Suzaku*, respectively) or inflow (for Fe XXVI, $v\sim 4500$ km s $^{-1}$) with velocities higher than what generally observed (Reynolds et al. 2004; Longinotti et al. 2007; but see also Bianchi et al. 2008 that detect an outflow of $v=900^{+500}_{-700}$ km s $^{-1}$). On the other hand, the high radiative efficiency of the source ($\eta=0.12$; Woo & Urry 2002) suggests that the accretion disc is stable down to the innermost regions around the BH, where the reflection component should be shaped by relativistic effects. For these reasons, although an outflowing emitting gas is not excluded, the broad line interpretation seems favoured. In fact, the profile of the line is compatible with being shaped by relativistic effects, consistent with its origin being in the surface of an accretion disc, in vicinity of a black hole. Nevertheless, the width of the line is not a compelling evidence. The observed broadening of the line can be reproduced also with the Comptonization process occurring in the upper layer of the ionized accretion disc. Moreover, we stress that the main evidences for the presence of a broad Fe K line comes from the mean summed spectrum. The process of summing spectra, although is a powerful way to extract information, might be dangerous in presence of spectral variability and when applied to observations taken many years apart. Thus, the final answer on the origin of these ionized lines will be obtained with either a higher resolution observation or with significantly longer *XMM-Newton* exposures.

6.3 Ionized Fe absorption lines

The *XMM-Newton* data indicate the presence of a highly ionized absorption component, the best fit column density being $N_H=5.8^{+5.2}_{-4.8}\times 10^{22}$ cm $^{-2}$ and ionization $\log(\xi)=5.15^{+1.25}_{-0.52}$. Moreover, fitting the absorption with this model, it results that the absorber has to be blueshifted by $0.0484^{+0.012}_{-0.013}$ c. The blueshift corresponds to an outflow velocity of ~ 14000 km s $^{-1}$. The structure implies a significant blueshift if the absorber is located in the core of Mrk 509 but, considering the systemic velocity of the galaxy, its energy is also consistent with a local absorber (McKernan et al. 2004; 2005; Risaliti et al. 2005; Young et al. 2005; Miniutti et al. 2007; but see also Reeves et al. 2008). Nevertheless, the observed vari-

ability between the *XMM-Newton* and *Suzaku* observations points towards an origin within Mrk 509.

An hint of variability is observed around 6.7 keV both in the *XMM-Newton* data and by comparing the *XMM-Newton* and *Suzaku* spectra. This could be due in principle to variability in the red wing of the ionized emission line. However, the total rms spectrum shows a peak of variability that is consistent with being narrow, thus it may suggest an alternative explanation. Indeed, the observed difference between the *XMM-Newton* and *Suzaku* Fe K line shapes could be due to a further ionized absorption component, present only the *XMM-Newton* observations, with a column density $N_H=5.4^{+4.8}_{-4.4}\times 10^{21}$ cm $^{-2}$ and ionization parameter $\log(\xi)=2.04^{+0.43}_{-0.60}$. When the structure at 6.7 keV is fitted with such a component, an absorption structure appears around 7.3 keV, nevertheless its equivalent width is not strong enough to reproduce the total absorption feature; moreover, it appears at slightly different energy, not completely fitting the ~ 7.3 keV line. Thus, the absorption structures at 6.7 and the one at 7.3 keV may be connected and they may be indicative of another absorption screen. If this further lower ionization absorption component is present, different absorption feature would be expected (due to the low ionization and high column density) at lower energies. Smith et al. (2007) analyzed the RGS data and detected two absorption components with physical parameters similar ($\log(\xi)=2.14^{+0.19}_{-0.12}$ and $3.26^{+0.18}_{-0.27}$; $N_H=0.75^{+0.19}_{-0.11}$ and $5.5^{+1.3}_{-1.4}\times 10^{21}$ cm $^{-2}$) to the ones that we infer, strengthening this interpretation. There is also evidence for another, higher ionization, mildly relativistic, and variable ionized component in the XMM data. The study of this more extreme component is addressed in another paper (Cappi et al., in preparation).

The observation of highly ionized matter in the core of Mrk 509 is in line with its high BH mass and accretion rate. In fact, we remind that at the Eddington limit the radiation pressure equals the gravitational pull, however the densities of the matter lowers with the BH mass (Shakura & Sunyaev 1976). Thus the ionization of the material surrounding high accretion rate and BH mass AGNs, such as Mrk 509, should be higher than normal. We stress, however, that in order to detail the physical parameters of the ionised emitter/absorber, further long observations are required.

7 CONCLUSIONS

The Fe K band of Mrk 509 shows a rich variety of emission/absorption components. The *XMM-Newton* and *Suzaku* data shows evidence for the presence of:

- a resolved, although not very broad, ($\sigma \sim 0.07$ keV) neutral Fe K α line and associated Fe K β emission. The width of the line suggests that the 6.4 keV line is produced in the outer part of the accretion disc (the broad line region or torus emission seem unlikely). The measured reflection fraction is consistent in this case with the intensity of the line, while a covering factor or column density higher than generally observed would be required if the line were produced in the BLR or the torus;
- both the *Suzaku* and the *XMM-Newton* data show an excess due to ionized Fe K emission. Both datasets show a superior fit when a broad ionized line coming from the central parts of the accretion disc is considered. The data are inconsistent with narrow emission from a distant scattering material at rest, while it can not be excluded if the gas is outflowing ($v\sim 3500$ km s $^{-1}$)
- both EPIC-pn and MOS data show an absorption line at ~ 7.3 keV, present in the summed spectrum of all *XMM-Newton* observations only. This component confirms the presence of highly ionized,

outflowing ($v \sim 14000 \text{ s}^{-1}$), gas along the line of sight. The comparison between *XMM-Newton* and *Suzaku* suggests a variability of this component;

- a hint of an enhancement of variability - both by considering the *XMM-Newton* data alone and by comparison between the two data sets - at $\sim 6.7 \text{ keV}$ that could be either due to the high variability of the red wing of the broad ionized Fe K line, possibly associated with a variation of the ionisation of the disc, or to a second ionized absorption line.

ACKNOWLEDGMENTS

This paper is based on observations obtained with *XMM-Newton*, an ESA science mission with instruments and contributions directly funded by ESA Member States and NASA. This work was partly supported by the ANR under grant number ANR-06-JCJC-0047. GP, CV and SB thank for support the Italian Space Agency (contracts ASI-INAF I/023/05/0 and ASI I/088/06/0). GM acknowledge funding from Ministerio de Ciencia e Innovación through a Ramón y Cajal contract. GP thanks Regis Terrier, Andrea Goldwurm and Fabio Mattana for useful discussion. We would like to thank the anonymous referee for the detailed reading of the manuscript and for the comments that greatly improved the readability of the paper.

REFERENCES

- Ashton, C. E., Page, M. J., Blustin, A. J., Puchnarewicz, E. M., Branduardi-Raymont, G., Mason, K. O., Córdova, F. A., & Priedhorsky, W. C. 2004, *MNRAS*, 355, 73
- Avni, Y. 1976, *ApJ*, 210, 642
- Basko, M. M. 1978, *ApJ*, 223, 268
- Bianchi, S., & Matt, G. 2002, *A&A*, 387, 76
- Bianchi, S., Balestra, I., Matt, G., Guainazzi, M., & Perola, G. C. 2003, *A&A*, 402, 141
- Bianchi, S., Matt, G., Balestra, I., Guainazzi, M., & Perola, G. C. 2004, *A&A*, 422, 65
- Bianchi, S., Matt, G., Nicastro, F., Porquet, D., & Dubau, J. 2005, *MNRAS*, 357, 599
- Bianchi, S., La Franca, F., Matt, G., Guainazzi, M., Jimenez Bailón, E., Longinotti, A. L., Nicastro, F., & Pentericci, L. 2008, *MNRAS*, 389, L52
- Costantini, E., et al. 2007, *A&A*, 461, 121
- Dadina, M., Cappi, M., Malaguti, G., Ponti, G., & de Rosa, A. 2005, *A&A*, 442, 461
- Davidson, K., & Netzer, H. 1979, *Reviews of Modern Physics*, 51, 715
- De Rosa, A., Piro, L., Matt, G., & Perola, G. C. 2004, *A&A*, 413, 895
- Dickey, J. M., & Lockman, F. J. 1990, *ARA&A*, 28, 215
- Goad, M., & Koratkar, A. 1998, *ApJ*, 495, 718
- Guainazzi, M., Bianchi, S., & Dovčiak, M. 2006, *Astronomische Nachrichten*, 327, 1032
- Haardt, F., Maraschi, L., & Ghisellini, G. 1997, *ApJ*, 476, 620
- Iwasawa, K., Miniutti, G., & Fabian, A. C. 2004, *MNRAS*, 355, 1073
- Leahy, D. A., & Creighton, J. 1993, *MNRAS*, 263, 314
- Longinotti, A. L., Bianchi, S., Santos-Lleo, M., Rodríguez-Pascual, P., Guainazzi, M., Cardaci, M., & Pollock, A. M. T. 2007, *A&A*, 470, 73
- Kaastra, J. S., Steenbrugge, K. C., Raassen, A. J. J., van der Meer, R. L. J., Brinkman, A. C., Liedahl, D. A., Behar, E., & de Rosa, A. 2002, *A&A*, 386, 427
- Kriss, G. A., et al. 2000, *ApJ*, 538, L17
- Magdziarz, P., & Zdziarski, A. A. 1995, *MNRAS*, 273, 837
- Malizia, A., Bassani, L., Zhang, S. N., Dean, A. J., Paciesas, W. S., & Palumbo, G. G. C. 1999, *ApJ*, 519, 637
- Maraschi, L., & Haardt, F. 1997, *IAU Colloq. 163: Accretion Phenomena and Related Outflows*, 121, 101
- Marziani, P., Sulentic, J. W., Zamanov, R., Calvani, M., Dultzin-Hacyan, D., Bachev, R., & Zwitter, T. 2003, *ApJS*, 145, 199
- Matt, G., Fabian, A. C., & Ross, R. R. 1996, *MNRAS*, 278, 1111
- McHardy, I. M., Papadakis, I. E., & Uttley, P. 1998, *The Active X-ray Sky: Results from BeppoSAX and RXTE*, 509
- McKernan, B., Yaqoob, T., & Reynolds, C. S. 2004, *ApJ*, 617, 232
- McKernan, B., Yaqoob, T., & Reynolds, C. S. 2005, *MNRAS*, 361, 1337
- Miller, L., Turner, T. J., Reeves, J. N., George, I. M., Kraemer, S. B., & Wingert, B. 2007, *A&A*, 463, 131
- Miniutti, G., et al. 2007, *PASJ*, 59, 315
- Molendi, S., Bianchi, S., & Matt, G. 2003, *MNRAS*, 343, L1
- Nandra, K. 2006, *MNRAS*, 368, L62
- Nandra, K., O'Neill, P. M., George, I. M., & Reeves, J. N. 2007, *MNRAS*, 382, 194
- Page, M. J., Davis, S. W., & Salvi, N. J. 2003, *MNRAS*, 343, 1241
- Palmeri, P., Mendoza, C., Kallman, T. R., Bautista, M. A., & Meléndez, M. 2003, *A&A*, 410, 359
- Palmeri, P., Mendoza, C., Kallman, T. R., & Bautista, M. A. 2003, *A&A*, 403, 1175
- Papadakis, I. E., Kazanas, D., & Akylas, A. 2005, *ApJ*, 631, 727
- Peterson, B. M., et al. 2004, *ApJ*, 613, 682
- Petrucci, P. O., et al. 2007, *A&A*, 470, 889
- Ponti, G., Cappi, M., Dadina, M., & Malaguti, G. 2004, *A&A*, 417, 451
- Ponti, G., Miniutti, G., Cappi, M., Maraschi, L., Fabian, A. C., & Iwasawa, K. 2006, *MNRAS*, 368, 903
- Pounds, K., Reeves, J., O'Brien, P., Page, K., Turner, M., & Nayakshin, S. 2001, *ApJ*, 559, 181
- Poutanen, J., & Fabian, A. C. 1999, *MNRAS*, 306, L31
- Reeves, J., Done, C., Pounds, K., Terashima, Y., Hayashida, K., Anabuki, N., Uchino, M., & Turner, M. 2008, *MNRAS*, 385, L108
- Reynolds, C. S., Brenneman, L. W., Wilms, J., & Kaiser, M. E. 2004, *MNRAS*, 352, 205
- Revnivtsev, M., Borozdin, K., & Emelyanov, A. 1999, *A&A*, 344, L25
- Revnivtsev, M., Sazonov, S., Jahoda, K., & Gilfanov, M. 2004, *A&A*, 418, 927
- Risaliti, G., Bianchi, S., Matt, G., Baldi, A., Elvis, M., Fabbiano, G., & Zezas, A. 2005, *ApJ*, 630, L129
- Ross, R. R., & Fabian, A. C. 2005, *MNRAS*, 358, 211
- Sazonov, S., Revnivtsev, M., Krivonos, R., Churazov, E., & Sunyaev, R. 2007, *A&A*, 462, 57
- Shakura, N. I., & Sunyaev, R. A. 1976, *MNRAS*, 175, 613
- Shih, D. C., Iwasawa, K., & Fabian, A. C. 2003, *MNRAS*, 341, 973
- Smith, R. A. N., Page, M. J., & Branduardi-Raymont, G. 2007, *A&A*, 461, 135
- Tombesi, F., de Marco, B., Iwasawa, K., Cappi, M., Dadina, M., Ponti, G., Miniutti, G., & Palumbo, G. G. C. 2007, *A&A*, 467, 1057
- Woo, J.-H., & Urry, C. M. 2002, *ApJ*, 579, 530
- Young, A. J., Lee, J. C., Fabian, A. C., Reynolds, C. S., Gibson,

- R. R., & Canizares, C. R. 2005, *ApJ*, 631, 733
Yaqoob, T., McKernan, B., Kraemer, S. B., Crenshaw, D. M.,
Gabel, J. R., George, I. M., & Turner, T. J. 2003, *ApJ*, 582, 105
Yaqoob, T., & Padmanabhan, U. 2004, *ApJ*, 604, 63
Zdziarski, A. A., Lubinski, P., & Smith, D. A. 1999, *MNRAS*,
303, L11
Zdziarski, A. A., Lubiński, P., Gilfanov, M., & Revnivtsev, M.
2003, *MNRAS*, 342, 355